ELSEVIER

Physica C 317–318 (1999) 312–319

PHYSICA C

The electronic structure of one- and two-dimensional cuprates from high-energy spectroscopy

R. Neudert [a], M.S. Golden [a,*], M. Knupfer [a], S. Haffner [a], J. Fink [a], S.-L. Drechsler [a], J. Málek [a], H. Rosner [a], R. Hayn [a], K. Ruck [a], G. Krabbes [a], W. Stephan [b], K. Penc [c], V.Y. Yushankhai [d], C. Waidacher [e], J. Richter [e], K.W. Becker [e], T. Osafune [f], N. Motoyama [f], H. Eisaki [f], S. Uchida [f]

[a] *Institut für Festkörper- und Werkstofforschung Dresden, PO Box 270016, D-01171 Dresden, Germany*
[b] *Department of Physics and Astronomy, University of Manitoba, Winnipeg, Manitoba, Canada R3T 2N2*
[c] *Service de Physique Théorique, CEA Saclay, 91191 Gif-sur-Yvette Cedex, France*
[d] *Joint Institute for Nuclear Research, 141980 Dubna, Russian Federation*
[e] *Institut für Theoretische Physik, TU Dresden, D-01062 Dresden, Germany*
[f] *Department of Superconductivity, The University of Tokyo, Bunkyo-ku, Tokyo 113, Japan*

Abstract

We report studies of the electronic structure and elementary excitations of undoped, one- and two-dimensional cuprates. Using high-energy spectroscopies such as X-ray absorption, photoemission and electron energy-loss spectroscopy, important information regarding the charge distribution, hole dynamics and dielectric response has been obtained. The comparison of the experimental data with suitable theoretical models sets constraints on the parameters entering into the model calculations.

Keywords: Electronic structure; One-dimensional cuprates; Two-dimensional cuprates

1. Introduction

There exist a wide variety of different 1D and 2D copper–oxygen networks built up of square-planar CuO_4 plaquettes, the best known representatives of which are the essentially 2D high-temperature superconductors (HTSC). Parallel to the study of the highly complex HTSC materials themselves, much can be learned regarding the physics of the cuprates by the high energy spectroscopic investigation of the elementary excitations of model, undoped cuprate networks. In the 2D systems, information of direct relevance to the extreme low doping regime of the HTSC can be gathered, while the 1D networks offer direct experimental access to low dimensional, correlated electron systems, bringing with it new physical concepts such as spin-charge separation.

In this contribution we give a brief overview of the insight that can be gained into the electronic structure of different 1D and 2D model cuprates using high-energy spectroscopy. The intention of this paper is to give an impression of the breadth over which pertinent information can be obtained, and thus due to space considerations some of the results

* Corresponding author. E-mail: golden@ifw-dresden.de

0921-4534/99/$ - see front matter
PII: S0921-4534(99)00074-X

presented, and particularly some of the theory, will have to be taken at face value. In general, we show that while the case of one dimension can be consistently understood within the framework of current models, the experimental data of the 2D networks still pose a considerable challenge to our theoretical understanding of the elementary excitations of the cuprates.

2. Discussion

Through the application of different high-energy spectroscopies, we can obtain the following information: (i) the hole distribution in the different cuprate networks using polarisation-dependent X-ray absorption spectroscopy (XAS); (ii) the dynamics of a single hole in the valence bands from angle-resolved photoemission (ARPES); additional information regarding hole delocalisation can also be derived from the screening response to the creation of a Cu $2p$ core-hole in photoemission (XPS); and (iii) the momentum-dependent dielectric response from electron energy-loss spectroscopy (EELS) in transmission.

It is clear that taken in combination, such high-energy spectroscopies offer a powerful probe of the electronic states close to the chemical potential, which control the physical properties of the compounds under consideration.

In Fig. 1 sketches of the different Cu–O networks studied here are presented. The straight chain built up of corner-sharing CuO_4 plaquettes (Fig. 1a) is best realised in Sr_2CuO_3, whereas in Li_2CuO_2 the plaquettes share their edges to form the chains (Fig. 1b). Suitable as representatives of 2D Cu–O networks are the CuO_2 (Fig. 1c) and Cu_3O_4 (Fig. 1d) planes of $Sr_2CuO_2Cl_2$ and $Ba_2Cu_3O_4Cl_2$, respectively. The former contains the CuO_2 planes familiar from the HTSC, while the latter contains Cu_3O_4 planes which are composed of two sub-systems: a Cu_AO_2 plane analogous to that of the HTSC, and an additional Cu_B site. The two sub-systems can be envisaged as a pair of interpenetrating 2D Heisenberg antiferromagnets, with quite different Néel temperatures: $T_N^A = 330$ K, $T_N^B = 31$ K. One of the deciding factors in the determination of the properties of such Cu–O networks are the geometry-controlled interaction angles between one copper atom and the next via the O atoms. For example, the 180° Cu–O–Cu superexchange interactions in Sr_2CuO_3 are responsible for antiferromagnetic ordering and strong coupling along the chains. In Li_2CuO_2, however, the Cu–O–Cu angle is close to 90°, resulting in ferromagnetic nearest neighbour interactions and weakly coupled plaquettes. Similarly, in $Ba_2Cu_3O_4Cl_2$ the low T_N^B reflects Cu_B's frustration with respect to the Cu_A spins as well as the low Cu_B–Cu_B exchange.

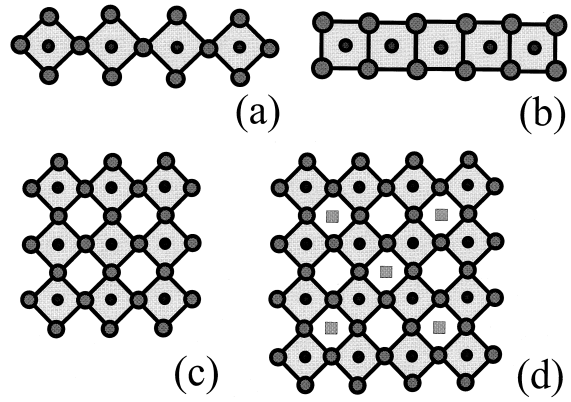

Fig. 1. Schematic representation of the 1D and 2D cuprate networks dealt with here. (a) The chain of corner-sharing plaquettes of Sr_2CuO_3; (b) the chain of edge-sharing plaquettes of Li_2CuO_2; (c) the CuO_2 plane of $Sr_2CuO_2Cl_2$; (d) the Cu_3O_4 plane of $Ba_2Cu_3O_4Cl_2$.

We start first with the 1D systems and the question of the hole distribution. In this context polarisation-dependent XAS is a well-established tool used to study the site and symmetry selective unoccupied electronic structure in cuprate-based materials [1]. Fig. 2 shows the O $1s$ XAS spectra for light polarisation within the CuO_4 plaquettes of Sr_2CuO_3. The a-axis lies parallel to the chain direction. We focus in the following on the features below 530.5 eV, which have their origin in the hybridisation of the O $2p_{x,y}$ orbitals with the (predominantly) Cu $3d_{x^2-y^2}$ derived upper Hubbard band (UHB). For $\boldsymbol{E}\|a$, the UHB-derived feature is centered at 529.6 eV, whereas for $\boldsymbol{E}\|b$ it is found at 529.1 eV. The two different peaks follow naturally from the two inequivalent oxygen sites of the CuO_3 chain structure, whereby the energetically lower peak is due to transitions into unoccupied states at the two peripheral O(2) sites and the higher lying peak to transitions at the central O(1) site [2]. Apart from their difference in energy,

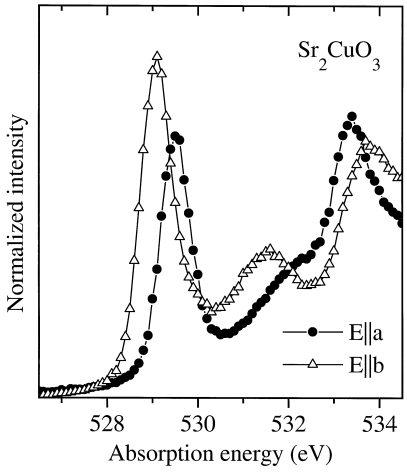

Fig. 2. O 1*s* X-ray absorption spectra of Sr_2CuO_3 for the electric-field vector $\boldsymbol{E}$ within the plane of the CuO_4 plaquettes. The *a*-axis corresponds to the chain direction.

the absorption maxima also differ in intensity. The O(1) site has two Cu neighbours compared to a single Cu neighbour for each of the O(2) sites. Correspondingly, as this O 1*s* XAS intensity is an expression of the hybridisation with the copper UHB, in the simplest picture one would expect twice the hole occupation for O(1) compared with O(2). Upon analysis of the peak areas, however, one finds a ratio for the hole occupation numbers, $n_{O(1)}/n_{O(2)} \approx 0.61$, instead of 0.5. Thus an additional influence is at work, which pushes the holes out towards the peripheral oxygen O(2) sites.

To examine the possible causes for this, we carried out calculations of the hole occupation numbers in the ground state within a standard four-band extended Hubbard model (see, e.g., Ref. [3]), which takes into account the chemical structure of the CuO_3 chain [2]. Although such a calculation necessarily has a number of parameters (whose interplay is, in some cases, complex) the following counteracting tendencies can be stated (hole picture): (i) while a higher on-site energy of the outer oxygen, i.e., $\Delta_{pp} = \varepsilon_{O(2)} - \varepsilon_{O(1)} > 0$, favors the central oxygen for hole occupation, and (ii) a non-zero intersite Coulomb interaction, V_{pd}, pushes the holes towards the outer oxygens O(2).

Thus, given the experimentally determined hole ratio of 0.61, as well as other experimental quantities for Sr_2CuO_3 such as the energy gap, *J*-value, etc., a detailed quantitative analysis within our four-band Hubbard model gives $V_{pd} \sim 2$ to 2.5 eV and $\Delta_{pp} \sim 0.5$ eV [2]. Thus, the nearest-neighbour Coulomb interaction, V_{pd}, is clearly enhanced in this paradigm 1D cuprate in comparison to the values accepted for the 2D cuprates ($V_{pd}^{2D} \leq 1$ eV [4]). Here, one sees that a relatively simple experimental quantity such as the O $2p$ hole ratio can give valuable information regarding the magnitude of an important model parameter which is difficult to extract from traditional sources such as the analysis of Cu $2p$ XPS spectra.

One step further than the question as to the location of the holes, is that of their dynamics. Recent ARPES experiments on 1D cuprates such as $SrCuO_2$ (Refs. [5,6]) and Sr_2CuO_3 (Ref. [7]) have been interpreted as indicating spin-charge separation, in which two features are observed, corresponding to the decay of the photohole into a holon and a spinon. The former disperses with a bandwidth related to the hopping term *t*, and the latter with a bandwidth governed by the exchange constant *J*. Besides in ARPES experiments, information regarding the delocalisation of holes in the valence band states can also be gained from investigating the screening response to the creation of a Cu $2p$ core-hole in high resolution photoemission. Fig. 3 shows the Cu $2p_{3/2}$ XPS

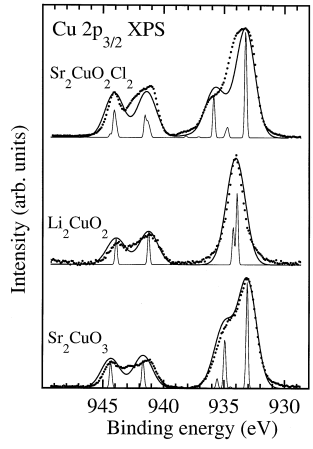

Fig. 3. Cu $2p_{3/2}$ core-level photoemission spectra of cleaved single crystals of $Sr_2CuO_2Cl_2$, Li_2CuO_2 and Sr_2CuO_3. Also shown as solid lines are the calculated spectra from a three-band Hubbard model [8], the results of which have either been broadened with a Gaussian of either 0.2 (to show the individual final states) or 1.8 eV (for direct comparison with experiment).

spectra of Sr_2CuO_3, Li_2CuO_2 and $Sr_2CuO_2Cl_2$. All spectra show, beside the so-called 'main line' at around 936 eV, a multiplet-split satellite feature between 945 eV and 950 eV. The satellite is due mainly to a final state in which the core hole is poorly-screened, i.e., Cu $\underline{2p}3d^9$, where $\underline{2p}$ denotes the core-hole. The main line then corresponds to a well-screened final state, generally denoted as Cu $\underline{2p}3d^{10}\underline{L}$. If this so-called 'ligand-hole' $\underline{L}$ delocalises, then a somewhat analogous situation to the injection of a single hole into the lowest lying electron removal states in an ARPES experiment is arrived at. In this way, the spectral profile of the Cu $2p$ photoemission main lines incorporates valuable information regarding the ease with which a ligand hole can delocalise in these systems.

We concentrate first on the 1D systems. Starting with the spectrum of Li_2CuO_2, we see that the main line is composed of a single component. In this case, the nature of the Cu $\underline{2p}3d^{10}\underline{L}$ final state is clear—as the plaquettes in this system are *edge* sharing, the ligand hole is localised predominantly on the four oxygen atoms surrounding the core-ionised copper site—the core-hole is locally screened [9]. This follows from the $\sim 90°$ Cu–O–Cu interaction angles, whereby hopping from one plaquette to its neighbour involves essentially orthogonal O $2p$ orbitals, and is thus reduced to such an extent that it is even smaller than the hopping to the next-nearest plaquette.

Also shown in Fig. 3 are calculated Cu $2p_{3/2}$ spectra for the different Cu–O networks based upon a three-band Hubbard model using a cumulant projection technique [8]. The advantage of this method is the treatment of infinite systems, thus circumventing some of the finite size problems which limit exact diagonalization studies. As can be seen from Fig. 3, the spectrum of Li_2CuO_2 can be very well reproduced by calculations based on an *isolated* CuO_4 plaquette, supporting the idea discussed above that only local screening is relevant for the main line in this compound. The model parameters required are $\Delta = 3.5$ eV, $t_{pd} = 1.3$ eV, $t_{pp} = 0.65$ eV, $U_{dc} = 8.5$ eV, $U_{dd} = 8.8$ eV [8].

In Sr_2CuO_3, the main line is clearly composed of two features, with the main component located at lower binding energies (BEs) than the locally screened final state in Li_2CuO_2. Once again, the geometry of the Cu–O network provides the clue to the screening channels available. The corner sharing plaquettes are linked to one another via a 180° Cu–O–Cu interaction path, thus favouring delocalisation of the ligand hole away from the core-ionised site, forming a Zhang–Rice singlet-like state on the neighbouring plaquette. Here, the calculated spectrum of an infinite chain also agrees well with experiment ($\Delta = 2.7$ eV, with other parameters as above), although interestingly a local antiferromagnetic spin order has to be imposed on the system to get the best agreement [8], despite the fact that the data were measured at room temperature and $T_N^{Sr_2CuO_3} = 5$ K. Examination of the theoretical hole distribution in the final state shows that the ligand hole has moved to the neighbouring plaquettes in the non-locally screened case, but has not delocalised further along the chain, in contrast to the results from exact diagonalisation [10]. The higher BE feature is a locally-screened final state, with the majority of the hole density located on the same plaquette as the core ionised copper [8]. Exact diagonalisation studies, however, predict that the hole density at the central chain O sites delocalises [10].

Thus, the comparison of simple experimental data with theoretical models allows valuable information to be gained not only as regards the delocalisation of holes in different 1D Cu–O networks, but also functions as a useful constraint on the parameters entering into the model calculations.

Moving beyond the single particle excitations discussed until now, EELS provides us with the energy and momentum dependent loss function $\mathrm{Im}(-1/\varepsilon(\boldsymbol{q}, \omega))$, and thus offers the possibility to study the dispersion of particle–hole excitations which is a two-particle response of the system [11].

The right panel of Fig. 4 shows the loss function of Sr_2CuO_3 measured for different momentum transfers q parallel to the chain direction. We focus on the loss function in the range 1.6 eV to $\sim$ 4 eV, as in this energy range the features are related to first possible interband transitions across the charge-transfer gap. The broad feature around 2.4 eV for $q = 0.08$ Å^{-1} narrows with increasing momentum transfer, evolving into a rather sharp peak at 2.8 eV for $q = 0.4$ Å^{-1}. At the zone boundary ($q = 0.8$ Å^{-1}) the excitation is centered at 3.2 eV. The study of the imaginary part of the density response function $N(q, \omega)$ of an extended one-band Hubbard

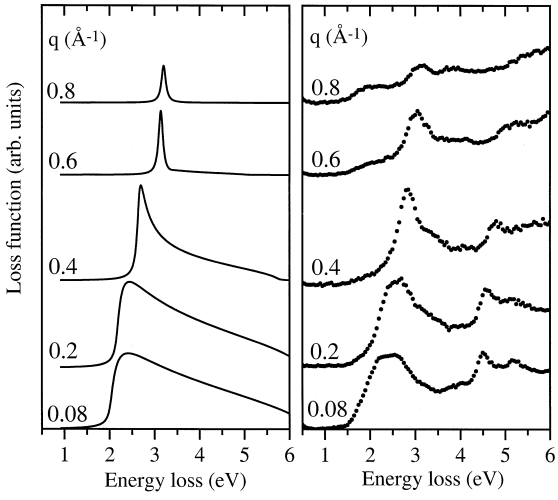

Fig. 4. Right panel: loss function of Sr_2CuO_3 measured with the momentum transfer $\boldsymbol{q}$ parallel to the chain direction. Left panel: calculated loss function within an extended one-band Hubbard model [12,13]. For details, see text.

model, including the nearest-neighbour Coulomb interaction V, qualitatively explains the anomalous narrowing of the low-energy peak with increasing momentum transfer [12]. Because of spin-charge separation which holds for this 1D model, it is possible to discuss a situation with no coupling of the carriers to the spin background. The loss function is proportional to $N(q, \omega)$, if the long-range Coulomb interaction $V_{3D}(q) = 4\pi e^2/q^2$ is also included. This has been done at the level of the random-phase approximation (RPA), leading to a renormalisation of the nearest neighbour interaction V in the short range interaction model [13].

The calculated loss function within this approach is shown in the left panel of Fig. 4 for parameters $t^{(1B)} = 0.55$ eV, $U^{(1B)} = 4.2$ eV, $V^{(1B)} = 1.3$ eV. Both the dispersion and the lineshape provide strong constraints on the parameters. The narrowing of the lowest energy loss feature with increasing q is well described within the theoretical approach and can be understood as mainly an effect of the intersite Coulomb interaction V. Its presence leads to an excitonic bound state between the created particle (double occupancy)–hole pair, which sharpens and lies below the continuum of interband transitions only for momentum transfers away from the centre of the Brillouin zone [13]. The value $V^{(1B)} = 1.3$ eV represents the unscreened value, since screening effects are treated in the RPA. For a short-range interaction model a smaller screened value of $V^{(1B)} \approx 0.8$ eV is appropriate.

Note that for a comparison between intersite Coulomb interactions in the XAS and EELS analyses presented here, V_{pd} in the multiband model denotes an interaction between neighbouring oxygen and copper atoms, while V in the effective one-band model corresponds to an *interplaquette*-type of interaction in the multiband model. With the expression $V^{(1B)} \sim n_d n_{p1} V_{pd} + n_d^2 V_{dd} + 2 n_{p1} n_{p2} V_{pp} + n_{p1}^2 \tilde{V}_{p1p1} + n_{p2}^2 \tilde{V}_{p2p2}$ (where the n's are occupation numbers), one can relate the intersite interactions of both models. With our XAS-derived value of $V_{pd} \sim 2.5$ eV, the first term yields $\approx 0.12 V_{pd} = 0.3$ eV. The value of $V^{(1B)} \approx 0.8$ eV can be approximately reproduced, if at least the second term is taken into account. Adopting for instance $V_{dd} \sim 0.9$ eV, we arrive at $V^{(1B)} \sim 0.6$ eV, in reasonable agreement with the results of the EELS data analysis.

Therefore, a consistent picture emerges from both the EELS and XAS of Sr_2CuO_3, whereby intersite Coulomb interactions play a significantly greater role than is true for the 2D cuprates. This may stem from the different screening in 1D and/or a different extension of the atomic wave functions due to the 1D confinement.

We now move on from the 1D to consider the 2D model cuprates. Due to the relevance to high temperature superconductivity, the dispersion relation of a single hole in the undoped CuO_2 plane of $Sr_2CuO_2Cl_2$ has attracted both a lot of experimental [14–16] and theoretical [17–19] attention. Due to the strong antiferromagnetic spin correlations in the undoped CuO_2 plane, the bandwidth of the quasiparticles resulting from injection of a hole via the photoemission process has been predicted to be proportional to the exchange constant J, rather than to the hopping term t. This point has been confirmed experimentally, as is illustrated in Fig. 5 which shows ARPES data for $Sr_2CuO_2Cl_2$, recorded along the $\Gamma \rightarrow (\pi,\pi)$ direction in the first Brillouin zone for different orientations of the polarisation vector of the synchrotron radiation with respect to the emission plane.

In the left panel, the plane in which photoelectron emission takes place is parallel to a mirror plane of

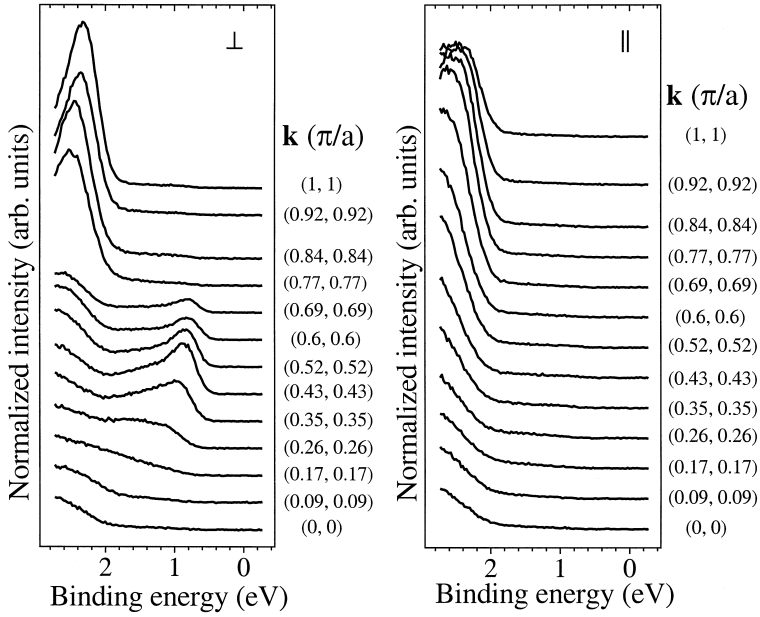

Fig. 5. Left panel: ARPES spectra of $Sr_2CuO_2Cl_2$ recorded along $\Gamma \rightarrow (\pi, \pi)$ with perpendicular polarisation. Right panel: the same experiment carried out with parallel polarisation. For details, see text.

the CuO_2 plane and the polarisation vector of the incoming synchrotron radiation is perpendicular to this plane. This corresponds to sampling initial states of odd symmetry with respect to the mirror plane. Under these conditions a clear dispersive feature is seen split off from the main valence band edge, having minimal BE and maximal intensity at $(\pi/2, \pi/2)$. Past this point it rapidly loses intensity as it disperses back up to higher energies. The 'bandwidth' between Γ and (π, π) is ca. 350 meV, both in keeping with previous studies [14–16] and theoretical predictions [17–19], giving a J-value of 0.17 ± 0.06 eV.

The right panel shows analogous measurements in which only the orientation of the polarisation vector of the synchrotron radiation has been altered to lie parallel to the emission/mirror plane, in this way sampling initial states of even symmetry. Now there is zero intensity for BEs up to 2 eV for all k-values. These results are consistent with the generally held opinion that the first electron-removal states in undoped 2D cuprates are Zhang–Rice singlets ZRSs, an antibonding combination of O $2p_{x,y}$ and Cu $3d_{x^2-y^2}$ orbitals, which have the correct symmetry to explain the observed strong polarisation dependence. It is interesting to note that the same type of polarisation-dependent experiment carried out along the $\Gamma \rightarrow (\pi,0)$ direction (not shown) shows more ARPES intensity at the energy corresponding to the ZRSs for odd than for even initial states, which is in contrast to the simple understanding of the ZRS symmetry discussed above. The reasons for this discrepancy are currently being investigated in detail.

As before, we can also gain information regarding hole delocalisation from the screening response in Cu $2p$ XPS. The spectrum of $Sr_2CuO_2Cl_2$ is also shown in Fig. 3. It is immediately clear that the main line is significantly broader than that of Sr_2CuO_3, and is comprised of at least three components. In this case, the calculated spectrum from the three-band Hubbard model manages to adequately describe both the low BE component of the main line and the shoulder at 936 eV (model parameters are $\Delta = 3.4$ eV, $t_{pd} = 1$ eV, $t_{pp} = 0.65$ eV, $U_{dc} = 7.7$ eV, $U_{dd} = 8.8$ eV) [8]. These two final states are related to non-locally and locally screened final states, respectively, the former corresponding to ZRS formation on plaquettes neighbouring the core-ionised site. However, it is clear that the model fails to predict the central component of the main line, located at ca.

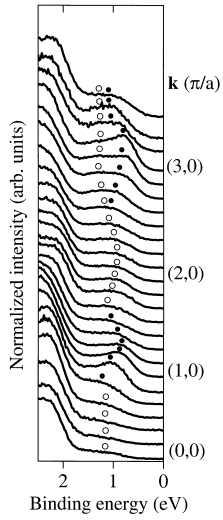

Fig. 6. Left panel: ARPES spectra of $Ba_2Cu_3O_4Cl_2$ recorded along $\Gamma \rightarrow (\pi, 0)$ with perpendicular polarisation. The filled (empty) symbols mark, as a guide to the eye, the energy positions of the ZRSs on the Cu_A (Cu_B) subsystems. For details, see text.

934 eV. Exact diagonalisation studies of clusters also encountered the same problem with the Cu $2p$ XPS spectrum of $Sr_2CuO_2Cl_2$ [20], indicating the presence of an additional screening channel not accounted for within the three-band Hubbard model, and therefore the necessity of extending the models to include, for example, apical, i.e., non-planar, orbitals.

Finally, we present ARPES measurements of hole dynamics in a 2D cuprate with a geometry deviating from the well-known CuO_2 case. $Ba_2Cu_3O_4Cl_2$ is a model, undoped cuprate which possesses Cu_3O_4 planes, as sketched in Fig. 1d. As also mentioned above, the two sub-systems into which this plane can be split have radically different T_N's, thus offering the unique possibility of investigating the dispersion of a single hole in both an antiferromagnetic and paramagnetic spin background simultaneously. Performing ARPES measurements at or slightly above room temperature, the hole can either be injected into the antiferromagnetically ordered Cu_A sublattice or the paramagnetic subsystem of the Cu_B spins.

In Fig. 6, we show a series of ARPES spectra of $Ba_2Cu_3O_4Cl_2$ recorded along the $\Gamma \rightarrow (\pi,0)$ direction (which is the analogous direction to $\Gamma \rightarrow (\pi,\pi)$ in $Sr_2CuO_2Cl_2$), with the polarisation geometry such that we are sensitive to initial states of odd symmetry with respect to the mirror plane which runs at 45° to the Cu–O bonds. Here the first electron removal states have lowest BE and greatest intensity at $(\pi,0)$ (and $(3\pi,0)$), which are the equivalent points to $(\pi/2, \pi/2)$ in $Sr_2CuO_2Cl_2$. However, after passing $(\pi, 0)$, their intensity does not fall away sharply as

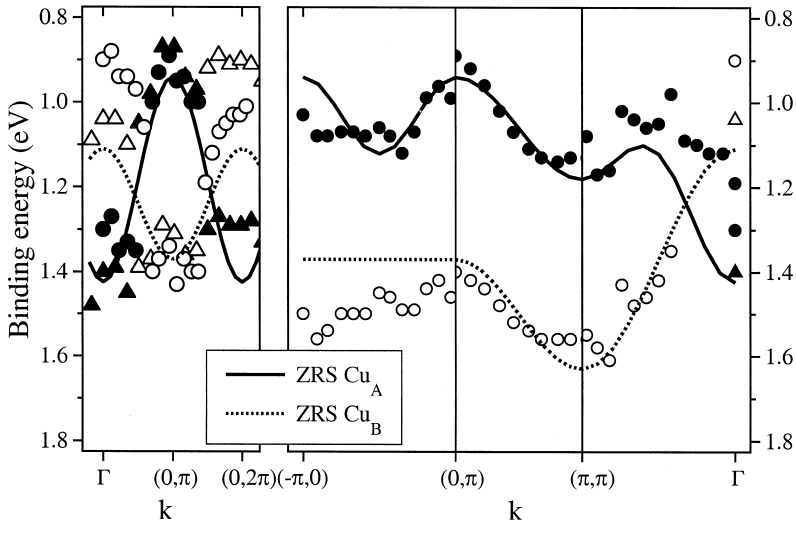

Fig. 7. Comparison of dispersion relations determined using ARPES of $Ba_2Cu_3O_4Cl_2$ (circles: 20 eV photon energy; triangles: 35 eV photon energy) with predicted ZRS dispersion relations for a 2D antiferromagnetic spin background (solid line) and a paramagnetic spin network (dotted line) [21]. For details, see text.

in $Sr_2CuO_2Cl_2$, but remains strong right up to $(3\pi, 0)$. This extra intensity is that of the photohole in the paramagnetic Cu_B sublattice, whereas the spectral weight at lowest BEs around $(\pi, 0)$ is that of the photohole in the antiferromagnetically ordered Cu_A sub-lattice. As these two contributions are not clearly separated in the experimental spectra, it is helpful to carry out model calculations to assist in the further interpretation of the data. This has been done within an extended t–J model, which takes into account the crucial role played by the spin background in determining the nature of the dispersion relation of the ZRSs created in the photoemission process [21].

Fig. 7 shows a plot of the experimentally observed peak positions (symbols), together with the predicted dispersion relations of a single hole in the Cu_A (solid line) or Cu_B (dotted line) sub-systems. The former results in a bandwidth governed by J, in analogy with the observed dispersion in the CuO_2 plane of $Sr_2CuO_2Cl_2$, giving an experimental J-value of 0.22 ± 0.03 eV, which is of the correct magnitude. The hole in the paramagnetic spin background, however, follows a tight-binding-like dispersion relation, with $t_B = -0.13 \pm 0.05$ eV [21]. In summary, as far as the spin background is concerned, the ARPES data from the Cu_3O_4 plane of $Ba_2Cu_3O_4Cl_2$ represent simultaneously both the low and very high doping limits in cuprate materials.

Our aim in this paper was to illustrate the wealth of information that can be obtained regarding the electronic structure and elementary excitations of 1D and 2D cuprates via their investigation with high energy spectroscopies such as XAS, XPS, ARPES, and EELS. We have shown that considerable insight can be gained not only into the charge distribution, hole dynamics and dielectric response of such systems, but also that the data serve as a source of constraints for the parameter-space available to model calculations developed to describe these highly correlated electron systems.

Acknowledgements

Financial support from the BMBF (13N 6599/9 and 05 605 BDA/05 SB8 BDA6), the DFG (SFB 463, Graduiertenkolleg 'Struktur und Korrelationseffekte in Festkörpern' der TU-Dresden), and the HCM program of the EU is gratefully acknowledged.

References

[1] J. Fink et al., J. Electron Spec. Rel. Phenom. 66 (1994) 395.
[2] R. Neudert et al., to be published.
[3] S.-L. Drechsler, J. Málek, H. Eschrig, Phys. Rev. B 55 (1997) 606.
[4] H. Eskes et al., Physica C 141 (1989) 424.
[5] C. Kim et al., Phys. Rev. Lett. 77 (1996) 4054.
[6] C. Kim et al., Phys. Rev. B 56 (1997) 15589.
[7] H. Fujisawa et al., Solid State Commun. 106 (1998) 543.
[8] C. Waidacher et al., preprint.
[9] T. Böske et al., Phys. Rev. B 57 (1998) 138.
[10] K. Okada et al., J. Phys. Soc. Jpn. 65 (1996) 1844.
[11] J. Fink, Adv. Electron. Electron Phys. 75 (1989) 121.
[12] W. Stephan, K. Penc, Phys. Rev. B 54 (1996) 17269.
[13] R. Neudert et al., Phys. Rev. Lett. 81 (1998) 657.
[14] B.O. Wells et al., Phys. Rev. Lett. 74 (1995) 964.
[15] S. LaRosa et al., Phys. Rev. B 56 (1997) 525.
[16] C. Kim et al., Phys. Rev. Lett. 80 (1998) 4245.
[17] E. Dagotto, Rev. Mod. Phys. 66 (1994) 763.
[18] A. Nazarenko et al., Phys. Rev. B 51 (1995) 8676.
[19] R.B. Laughlin, Phys. Rev. Lett. 79 (1997) 1726.
[20] T. Böske et al., Phys. Rev. B 56 (1997) 3438.
[21] M.S. Golden et al., Phys. Rev. Lett. 78 (1997) 4107.